Cross section of the impact single ionization of B^{2+} by H^{+}*

Ye Dan-Dan(叶丹丹), Qi Yue-Ying(祁月盈)†, Hu Ya-Hua(胡亚华), and Ning Li-Na(宁丽娜)

College of Mathematics, Physics and Information Engineering, Jiaxing University, Jiaxing 314001, *China*

(Received 16 September 2012; revised manuscript received 22 December 2012)

The ionization process of B^{2+} by H^{+} impact is studied using the continuum-distorted-wave eikonal-initial-state (CDW-EIS) method and the modified free electron peak approximation (M-FEPA), respectively. Total, single-, and double-differential cross sections from 1s and 2s orbitals are presented for the energy range from 10 keV/u to 10 MeV/u. Comparison between the results from the two methods demonstrates that the total and single-differential cross sections for the high-energy incident projectile case can be well evaluated using the simple M-FEPA model. Moreover, the M-FEPA model reproduces the essential features of the binary-encounter (BE) bump in the double-differential cross sections. Thus, the BE ionization mechanism is discussed in detail by adopting the M-FEPA model. In particular, the double- and single-differential cross sections from the 2s orbital show a high-energy hip, which is different from those from the 1s orbital. Based on Ref. [1], the Compton profiles of B^{2+} for 1s and 2s orbitals are given, and the hips in DDCS and SDCS from the 2s orbital are explained.

Keywords: continuum-distorted-wave eikonal-initial-state (CDW-EIS) method, modified free electron peak approximation (M-FEPA), binary-encounter (BE) bump, Compton profile

PACS: 34.10.+x, 34.50.–s **DOI:** 10.1088/1674-1056/22/5/053401

1. Introduction

Ion–atom collision ionization plays a vital role in basic research and various fields of applied physics, such as plasma physics, astrophysics, and radiation physics. Hence, understanding the basic atomic ionization processes has practical as well as fundamental physical importance. In the past decades, great progress has been made in this active field,[2–4] and various theoretical approaches have been developed to describe the whole energy spectrum of emitted electrons: the first-order Born approximation (FBA)[5] (restricted to high-energy projectile collision), classical trajectory Monte Carlo (CTMC)[6] (suitable for moderate- and high-energy projectile collision), atomic orbital close-coupling (AOCC)[7–9] (suitable for low- and moderate-energy projectile collision), continuum-distorted-wave (CDW)[10] (suitable for high-energy projectile collision), and the continuum-distorted-wave eikonal-initial-state (CDW-EIS) method[11] (suitable for moderate- and high-energy projectile collision). Particularly, the CDW-EIS method is an evolution of the CDW approximation, in which the perturbation in the initial state is replaced by the Eikonal approximation.[12] Previous studies have demonstrated that the CDW model fails for intermediate impact energies due to the lack of normalization of the initial state. The CDW-EIS model for ion-atom collision ionization process shows good agreement with the experimental data of the total cross section over a wide range of emitted electronic energy. As shown in Refs. [13] and [14], the total ionization cross sections for the process H^{+}+Li were calculated within the energy range from 10 keV/u to 10 MeV/u using CDW-EIS model, which are in good agreement with the experimental data, so the similar CDW-EIS approximation is adopted in our present work. In addition, many ionization mechanisms have been also found: soft collision (SC) (the low-energy peak),[15] electron captures to the continuum (ECC) (the cusp-shaped peak),[16] binary encounter (BE) (the high-energy ejected electrons),[17] and saddle ionization.[18] The center picture has been recognized as a useful concept[19] for understanding various ionization mechanisms. (i) The SC mechanism, which is characterized by small energy and momentum transfers involving weak projectile impact, is associated with the target–center case, and the FBA can well describe the SC ionization because it includes the full target interaction in the final state. (ii) The ECC mechanism can be successfully explained by means of the CDW and CDW-EIS approaches, because the ECC implies two-center phenomena, where the long-range forces of both the incident particle and target atoms play an important role in the formation of the electron cusp where the velocity of the emitted electron is close to that of the projectile. (iii) The BE mechanism, which is characterized by a large momentum transfer, can be referred to as the zero-center case, and it can be described by the free-electron peaking approximation (FEPA).[16] In this work, in order to well account for the BE ionization, we also exhibit the modified free electron peak approximation (M-FEPA).

In our work, we focus on the ionization process of Boron ion by proton impact. Boron element is the adopted plasma facing material in the International Thermonuclear Experi-

*Project supported by the National Basic Research Program of China (Grant No. 2013CB922200) and the National Natural Science Foundation of China (Grant Nos. 11005049, 11025417, 10979007, and 10974021).

†Corresponding author. E-mail: qi_yying@yahoo.com.cn

© 2013 Chinese Physical Society and IOP Publishing Ltd

mental Reactor (ITER), because it can be rapidly ionized and does not contribute to radiative losses in the central plasma core. Enhanced energy confinement in current tokamak experiments has been achieved by coating heavy metal facing components with boron.[20] Besides, boronization is a widely used strategy in carbon-based plasma facing components to improve their erosion, hydrogen retention, and some thermo-mechanical properties.[21] Thus, a collision process involving boron atoms (ions) has attracted increasing attention.[22,23] Hydrogen isotopes are magnetic confinement and inertial controlled fusion (ICF) fuel.[20] In the ICF experiments, the heated high-energy protons easily interact with wall materials, so the following collision process:

$$\mathrm{H}^{+}+\mathrm{B}^{2+}=\mathrm{H}^{+}+\mathrm{B}^{3+}+\mathrm{e} \tag{1}$$

has important significance in laboratory research. However, as far as we know, the only available datum of ionization for the system B^{2+}+H and the process $\mathrm{e}+\mathrm{B}^{2+}$ can be found in Refs. [21] and [24]. Recently, absolute measurement of the K-shell photo-ionization cross sections of ground-state B^{2+} has been performed.[25] The Coulomb–Born approximation has been employed to study charge transfer process for B^{q+} (q = 1–4) with H.[26,27] The cross sections of the charge exchange for B^{q+} (q = 1–5) with H have been systematically studied by adopting the CTMC method.[28] However, the data of the cross sections for electron excitation, capture, and ionization during the collision process of H^{+}+B^{2+} are seldom in theoretical and experimental studies.

The rest of the paper is organized as follows. The adopted theoretical method is briefly outlined in Section 2. The calculated results and the discussion of ionization mechanisms are presented in Section 3. At last, a summary is given. Atomic units will be used in the remaining part of this article, unless explicitly indicated.

2. Theoretical method

In the CDW-EIS calculations, the ion–atom collision ionization is usually treated as a three-body problem. The independent-electron model is adopted for multi-electronic targets. That is to say, the passive electrons are assumed to be frozen during the collision process. Based on the impact parameter treatment, the nuclear orbit is treated as classical rectilinear, while the electrons are completely described by adopting the quantum method. The cross section can be obtained by means of integral for the transition probability, which is described by the scattering matrix elements. The differences between various theoretical methods lie in the selection of the initial and final wave functions for the collision systems, and those of interaction potentials.

As shown in Fig. 1, we consider the impact ionization process of a lithium-like boron ion target (T) with the effective charge $\widetilde{Z}_{\mathrm{T}}$ by the projectile (P) with the nuclear charge Z_{P} and velocity $\boldsymbol{\upsilon}_{\mathrm{P}}$. In addition, $\boldsymbol{\rho}$ is the impact parameter ($\boldsymbol{\rho}\cdot\boldsymbol{\upsilon}_{\mathrm{P}}=0$), $\boldsymbol{R}$ is the position vector of the projectile relative to the target ($\boldsymbol{R}=\boldsymbol{\rho}+\boldsymbol{\upsilon}_{\mathrm{P}}t$), $\boldsymbol{r}_{\mathrm{P}}$ and $\boldsymbol{r}_{\mathrm{T}}$ are the position vectors of the electron measured from the nuclei of projectile and target, respectively; and $\boldsymbol{r}=(\boldsymbol{r}_{\mathrm{T}}+\boldsymbol{r}_{\mathrm{p}})/2$. In the CDW-EIS approximation, the transition amplitude can be written as[29]

$$a_{\mathrm{if}}(\boldsymbol{\rho})=-\mathrm{i}\int_{-\infty}^{\infty}\mathrm{d}t\left\langle \Psi_{\mathrm{i}}^{+}\left|\hat{H}_{\mathrm{e}}-\mathrm{i}\frac{\partial}{\partial t_r}\right|\Psi_{\mathrm{f}}^{-}\right\rangle. \tag{2}$$

The initial wave function in the following form:[11,12]

$$\begin{aligned}\Psi_{\mathrm{i}}^{+}(\boldsymbol{r},t) &= \phi_{\mathrm{i}}(\boldsymbol{r}_{\mathrm{T}})\exp(-\mathrm{i}\varepsilon_{\mathrm{i}}t)\exp\left(-\frac{1}{2}\mathrm{i}\boldsymbol{\upsilon}_{\mathrm{P}}\cdot\boldsymbol{r}-\frac{1}{8}\mathrm{i}\upsilon_{\mathrm{P}}^{2}t\right)\\ &\quad\times\exp\left(-\mathrm{i}\upsilon_{\mathrm{P}}\ln(\upsilon_{\mathrm{P}}r_{\mathrm{P}}+\boldsymbol{\upsilon}_{\mathrm{P}}\cdot\boldsymbol{r}_{\mathrm{P}})\right),\end{aligned} \tag{3}$$

is chosen $\phi_{\mathrm{i}}(\boldsymbol{r}_{\mathrm{T}})\exp(-\mathrm{i}\varepsilon_{\mathrm{i}}t)$ is the initial normalized wave function of the bound electron with the bound energy ε_{i}. For the present B^{2+} target, $\phi_{\mathrm{i}}(\boldsymbol{r}_{\mathrm{T}})$ employs the Roothan–Hatree–Fock wave function;[30] $\exp(-\mathrm{i}\boldsymbol{\upsilon}_{\mathrm{P}}\cdot\boldsymbol{r}/2-\mathrm{i}\upsilon_{\mathrm{P}}^{2}t/8)$ is the electron translation factor,[31] which takes account of the energy and momentum associated with the translation motion of the active electron; and $\exp\left(-\mathrm{i}\upsilon_{\mathrm{P}}\ln(\upsilon_{\mathrm{P}}r_{\mathrm{P}}+\boldsymbol{\upsilon}_{\mathrm{P}}\cdot\boldsymbol{r}_{\mathrm{P}})\right)$ is the initial eikonal distortion factor,[12] which describes the electron in a continuum state of the projectile. The final wave function can be expressed as[11,12]

$$\begin{aligned}\Psi_{\mathrm{f}}^{-}(\boldsymbol{r},t) &= (2\pi)^{3/2}\exp(\mathrm{i}\boldsymbol{k}\cdot\boldsymbol{r}_{\mathrm{T}})\exp(-\mathrm{i}\varepsilon_{\mathrm{k}}t)\\ &\quad\times\exp\left(-\frac{1}{2}\mathrm{i}\boldsymbol{\upsilon}_{\mathrm{P}}\cdot\boldsymbol{r}-\frac{1}{8}\mathrm{i}\upsilon_{\mathrm{P}}^{2}t\right)\\ &\quad\times N^{*}(\xi)\,{}_1\mathrm{F}_1\left(-\mathrm{i}\xi;1;-\mathrm{i}(kr_{\mathrm{T}}+\boldsymbol{k}\cdot\boldsymbol{r}_{\mathrm{T}})\right)\\ &\quad\times N^{*}(\zeta)\,{}_1\mathrm{F}_1\left(-\mathrm{i}\zeta;1;-\mathrm{i}(pr_{\mathrm{P}}+\boldsymbol{p}\cdot\boldsymbol{r}_{\mathrm{P}})\right).\end{aligned} \tag{4}$$

The vector $\boldsymbol{k}(\boldsymbol{p}=\boldsymbol{k}-\boldsymbol{\upsilon}_{\mathrm{P}})$ is the momentum of the emitted electron seen from the center of mass of the target (projectile); $\varepsilon_{\mathrm{k}}=k^{2}/2$, $\xi=\widetilde{Z}_{\mathrm{T}}/k$, $\zeta=Z_{\mathrm{P}}/p$; $N(a)$ is the Coulomb density of states defined by $N(a)=\exp(\pi a/2)\Gamma(1-\mathrm{i}a)$; the quantity $(2\pi)^{3/2}\exp(\mathrm{i}\boldsymbol{k}\cdot\boldsymbol{r}_{\mathrm{T}})\exp(-\mathrm{i}\varepsilon_{\mathrm{k}}t)$ is the normalized free electron wave function relative to the target; and

$$\begin{aligned}&N^{*}(\xi)\,{}_1\mathrm{F}_1\left(-\mathrm{i}\xi;1;-\mathrm{i}(kr_{\mathrm{T}}+\boldsymbol{k}\cdot\boldsymbol{r}_{\mathrm{T}})\right)\\ &\left(N^{*}(\zeta)\,{}_1\mathrm{F}_1\left(-\mathrm{i}\zeta;1;-\mathrm{i}(pr_{\mathrm{P}}+\boldsymbol{p}\cdot\boldsymbol{r}_{\mathrm{P}})\right)\right)\end{aligned}$$

gives the distorted factors of emission electron by the target (the projectile). The electronic Hamiltonian is

$$\hat{H}_{\mathrm{e}}=-\frac{1}{2}\nabla_{r}^{2}-\frac{Z_{\mathrm{T}}}{r_{\mathrm{T}}}-\frac{Z_{\mathrm{P}}}{r_{\mathrm{P}}}+\frac{Z_{\mathrm{P}}Z_{\mathrm{T}}}{R}. \tag{5}$$

The inter-nuclear potential has been removed by a phase transformation,[32] which does not contribute to the cross section. Thus, the triply-differential cross section is given by

$$Q(\boldsymbol{k})=\frac{\mathrm{d}^{3}\sigma}{\mathrm{d}\boldsymbol{k}}=\frac{\mathrm{d}^{3}\sigma}{k^{2}\,\mathrm{d}k\,\mathrm{d}\Omega}=\int\mathrm{d}\boldsymbol{\rho}|a_{\mathrm{if}}(\boldsymbol{\rho})|^{2}. \tag{6}$$

The double-differential, single-differential, and total cross sections can be written as

$$\sigma(\varepsilon_k,\theta)=\frac{d^2\sigma}{d\varepsilon_k d(\cos\theta)}=k\int_0^{2\pi}d\phi Q(\boldsymbol{k}), \tag{7}$$

$$\begin{cases}\sigma(\varepsilon_k)=\dfrac{d\sigma}{d\varepsilon_k}=\displaystyle\int d\theta\sin\theta\sigma(\varepsilon_k,\theta),\\ \sigma(\theta)=\dfrac{d\sigma}{d(\cos\theta)}=\displaystyle\int d\varepsilon_k\sigma(\varepsilon_k,\theta),\end{cases} \tag{8}$$

$$\sigma=\int_0^{\pi}d\theta\sin\theta\sigma(\theta)=\int_0^{\infty}d\varepsilon_k\sigma(\varepsilon_k), \tag{9}$$

respectively.

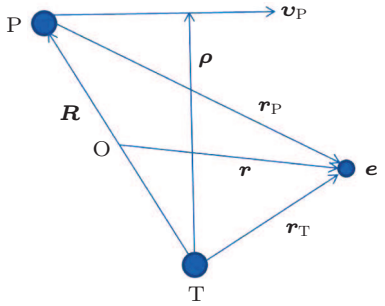


Fig. 1. (color online) Coordinates for proton (P) collision with B^{2+} (T). The origin O is taken as the midpoint of the inter-nuclear line.

In the present work, we also consider the results of FEPA, because the comparison between CDW-EIS and FEPA data may be very useful for evaluating and understanding electron emission ionization mechanisms. In the FEPA calculation, the electron is described by the bound wave function of the target in the entrance channel, and the outgoing electron is treated as a simple plane wave, as the three particles in the exit channel are all free (which is defined by the zero-center case). The double-differential cross section in FEPA[33] is

$$\frac{d\sigma^2}{d\varepsilon_k d\Omega}=\frac{4Z_P^2}{\upsilon_P^2k^3}J(p_z), \tag{10}$$

where $J(p_z)$ is the Compton profile determined by the initial momentum distribution along the incident beam direction in the following form:

$$p_z=k\cos\theta-\frac{k^2}{2\upsilon_P}-\frac{\varepsilon_i}{\upsilon_P}. \tag{11}$$

The expression of the Compton profile $J(p_z)$ is available in Ref. [1]. In order to remove the singularity for $k\to 0$ in Eq. (10), we have replaced the momentum k by k_c[19]

$$k_c=\left(2\varepsilon_k+3\varepsilon_i\left(\ln\frac{\upsilon_P^2}{\varepsilon_i}\right)^{-2/3}\right)^{1/2}. \tag{12}$$

Based on the first-order Born approximation results[5] when $k\to 0$, this semi-empirical expression may well predict the SC ionization, which will be discussed in the next subsection. Hence, the FEPA method is named M-FEPA in our paper. The single-differential and total cross sections are expressed as [19]

$$\frac{d\sigma}{d\varepsilon_k}=\frac{8\pi Z_P^2}{\upsilon_P^2k_c^4}, \tag{13}$$

$$\sigma=\frac{4\pi Z_P^2}{3\varepsilon_i\upsilon_P^2}\left(\ln\frac{\upsilon_P^2}{\varepsilon_i}\right)^{2/3}, \tag{14}$$

respectively.

3. Results and discussion

The present approximations are based on the independent electron model, so all of the cross sections should have been gained by multiplying the number of electrons in the shell considered. However, we only give the case of one electron emission. Results are presented as follows. Firstly, in order to well understand the ionization mechanism, the bound wave functions and the Compton profiles of B^{2+} are shown.

The bound wave functions of B^{2+} are shown in Fig. 2(a). As we all known, the wave function of 1s orbital has no node and is almost localized close to the nucleus ($r<1$ a.u.); the wave function of 2s orbital has one node, and thus the curve is divided into two parts: the inner part close to the nucleus ($r<0.5$ a.u.) and the outer part far from the nucleus (0.5 a.u. $<r<6$ a.u.).[28] The differences between the two wave functions of B^{2+} may affect the Compton profiles. As seen in Fig. 2(b), the line shape of the 1s orbital is broader, which can be explained by the uncertainty principle: the distribution of momentum can be wider because the 1s orbital is confined close to the nucleus. While the line shape of the 2s orbital also has two parts as its wave function does: the central peak is governed by the outer distribution (0.5 a.u. $<r<6$ a.u.) and the inner distribution ($r<0.5$ a.u.) contributes to the line shape of the broad background, as explained in Ref. [34]. It is also noted that the hips appear in the vicinity of $|p_z|=2$ a.u. in the Compton profiles of the 2s orbital, which should originate from the node of wave function for the orbital 2s. In the following, the hips will be found in the double-differential cross sections and even in single-differential cross sections.

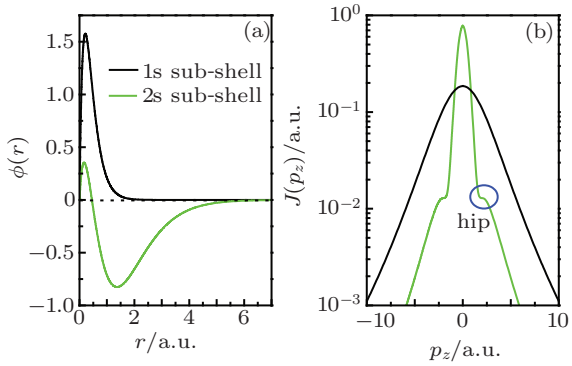


Fig. 2. (color online) (a) Bound wave functions of B^{2+}. (b) The Compton profiles of B^{2+} based on Ref. [1].

3.1. Double-differential cross sections (DDCS)

DDCS about the ejected electron energy and the ejected electron angle can be obtained from Eq. (7) (CDW-EIS) and Eq. (10) (M-FEPA), respectively. Here, in order to discuss the ionization mechanisms conveniently, we only plot DDCS for a fixed electron ejection angle $\theta = 0^\circ$ with the incident projectile energies $E_P = 500$ keV/u and $E_P = 5000$ keV/u, as shown in Fig. 3. The DDCS derived from the CDW-EIS method all exhibit three obvious structures except for that from 1s sub-shell for $E_P = 500$ keV/u (only the ECC peak is found clearly): SC peak (~ 0 eV), ECC peak (~ 272 eV for $E_P = 500$ keV/u, which can be obtained by setting $v_P = k$), and BE bump (~ 1014 eV for $E_P = 500$ keV/u and the 2s orbital, which can be obtained from Eq. (15)). This demonstrates that the CDW-EIS model can well reveal the three ionization mechanisms, where the two-center case is accounted for. However, for the results obtained using the M-FEPA method, the SC and BE ionization mechanisms can be reasonably described, but the ECC ionization cannot be given when introducing the semi-empirical expression (12) and describing the zero-center case. As seen from Fig. 3, the ECC peaks do not exist in the results obtained using the M-FEPA method. In addition, the result obtained using the CDW-EIS method from1s orbital for the moderate projectile energy $E_P = 500$ keV/u (corresponding to $v_P \approx 4.472$ a.u., which is close to the averaged velocity $\bar{v}_e$ of the initial bound electron relative to the target, $\bar{v}_e \approx \sqrt{2\varepsilon_i} = 4.197$ a.u.) denotes that the ECC ionization makes a dominant contribution, and there are not obvious SC and BE ionization. With the collision energy increasing, SC and BE ionization become more and more important. It is also shown that the M-FEPA results from 1s orbital for the moderate projectile energy $E_P = 500$ keV/u does not show obvious SC and BE ionization. Moreover, DDCS resulting from the two models have great deviations because the ECC ionization plays an important role in this case. With the collision energy increasing, SC and BE ionization appear, as seen in Fig. 3 (M-FEPA). Furthermore, for SC ionization, although the results of M-FEPA model have great differences from that of CDW-EIS model in DDCS, they are in excellent agreement in the single-differential cross sections, which is verified in the next subsection. While for BE bump, the results of M-FEPA model show good agreement with those of CDW-EIS model, especially for the higher incident projectile energy (when $E_P = 5000$ keV/u for 2s orbital). Therefore, the M-FEPA model can well describe the essential features of BE bump in DDCS. As shown in Fig. 3, it is also noted that, the DDCS from the 2s orbital exhibits the hips, which are different from those from the 1s orbital. This may be explained as follows: Eq. (10) describes a remarkable peak which is identified as the BE peak related to the Compton profile maximizes at $p_z = 0$. Thus, the location of the electron energy at BE maximum can be obtained using Eq. (11), as it was in Ref. [35].

$$E_k^{BE} = 2v_P^2 \cos\theta - 2\varepsilon_i. \tag{15}$$

Besides, according to Eq. (10), with the electron momentum k increasing, DDCS decreases, which results in the asymmetry of the BE bump, and the hips should come from the Compton profiles of B^{2+} for the 2s orbital (see Fig. 2(b)). Thus, the structure analysis of BE bump may be performed by means of the M-FEPA model.

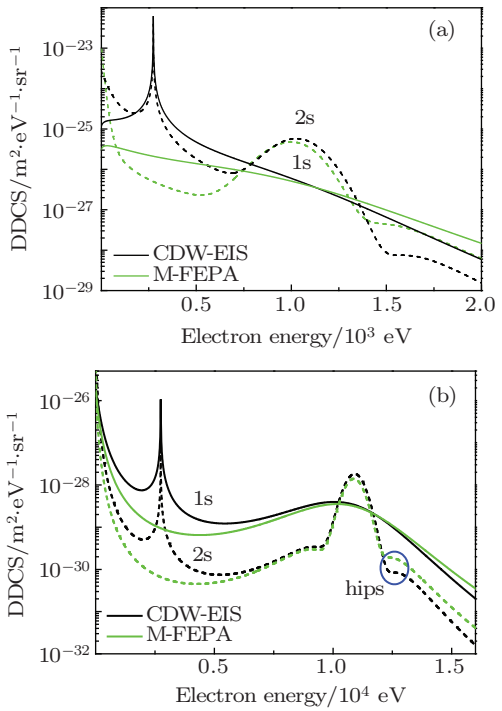


Fig. 3. (color online) Double-differential cross sections of 1s and 2s electrons as a function of electron energy with $\theta = 0^\circ$ for (a) $E_P = 500$ keV/u and (b) $E_P = 5000$ keV/u. Short-dashed line: 2s sub-shell; solid line: 1s sub-shell; blue circle: the shape of curve is defined as the 'hip'.

3.2. Single-differential cross sections (SDCS)

The SDCS with respect to the ejected electron energy for the projectile with $E_P = 500$ keV/u and $E_P = 5000$ keV/u can be obtained using Eq. (8) (CDW-EIS) and Eq. (13) (M-FEPA), respectively. Equation (13) (M-FEPA) is a similar expression which has previously been deduced from the classical Rutherford cross section[19] only using k instead of k_c. According to the classical conservation rules of energy and momentum, $\varepsilon_k = 4T$ (T is the kinetic energy of the electron with the same velocity as the projectile one) is the maximum energy that the free electron can gain from the incident proton.[36] Thus, it is reasonable to set $d\sigma/d\varepsilon_k = 0$ (Eq. (13)) when $\varepsilon_k > 4T$, as seen in Fig. 4 (M-FEPA). When $\varepsilon_k < 4T$, the results from CDW-EIS and M-FEPA models are in good agreement for all high incident projectile energies (except for the result from 1s sub-shell for $E_P = 500$ keV/u). Thus, the SDCS for B^{2+} impacted by H^+ with high energy and for $\varepsilon_k < 4T$ can be well estimated

by the simple M-FEPA model. When $\varepsilon_k > 4T$, the curve for the theoretical results from CDW-EIS method exhibits a turning point. For the high-energy projectile incident, the position of the turning point is the BE peak ($\varepsilon_k \approx 4T$ is obtained from Eq. (15)), and then the curve declines sharply, especially for the higher incident proton energy, as seen in Fig. 4(a) (CDW-EIS). This phenomenon is consistent with the results of the classical conservation rules of energy and momentum as mentioned above. For the moderate-energy projectile incident (for the ionization from 1s orbital with $E_P = 500$ keV/u), the position of the turning point is the ECC peak ($\varepsilon_k \approx T$), which demonstrates that the ECC ionization makes a relatively important contribution in this case. Hence, it can be seen that the SDCS derived from M-FEPA has great difference from the result of CDW-EIS. This is related to the characteristics of the M-FEPA model, as discussed above.

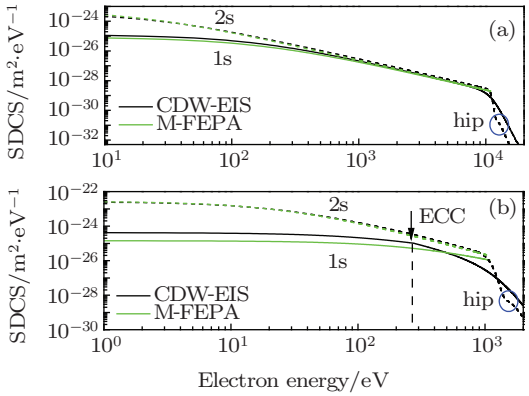


Fig. 4. (color online) Single-differential cross sections for electron emission with impact energy of (a) $E_P = 5000$ keV/u (b) $E_P = 500$ keV/u. Short dashed line: 2s sub-shell; solid line: 1s sub-shell; blue circle: the shape of curve is defined as 'hip'; and black arrows indicate the positions of ECC.

It is interesting to analyze Fig. 4(a), and two phenomena are found: (i) the curves of SDCS from the 1s and 2s sub-shells almost overlap in the higher ejected electron energy; (ii) SDCS from 2s sub-shell shows a high-energy hip, which is different from that for 1s sub-shell. These can be illustrated by Fig. 5. By adopting CDW-EIS, the double-differential cross sections for the different angles and SDCS as functions of emitted electron energy from 2s sub-shell when $E_P = 500$ keV/u are displayed, as shown in Fig. 5. The electron energy of the BE peak decreases with increasing electron emission angle, and the peak disappears when the ejected electron angle is close to 90°. Therefore, it is clearly noted that the higher-energy ejection electrons mainly come from the BE mechanism corresponding to the large momentum transfer. In this case, the ionization cross sections will be weakly dependent on the initial conditions of the bound electron in the target. Thus, the agreement of SDCS from the 1s and 2s sub-shells at higher ejected electron energy is explained. The high-energy hip in the SDCS from the 2s sub-shell comes from the node of the 2s wave function, as explained in Section 3.1.

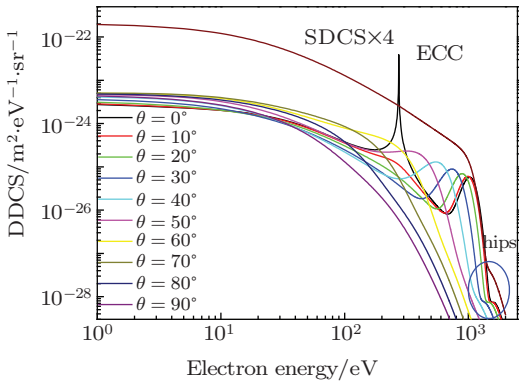


Fig. 5. (color online) Double-differential cross sections at different angles and single-differential cross section of the 2s sub-shell for $E_P = 500$ keV/u. In order to show the SDCS clearly, the SDCS is multiplied by 4.

3.3. Total cross sections (TCS)

Due to the lack of experimental data for the $H^+ + B^{2+}$ system, the CDW-EIS method is used to calculate the total ionization cross sections for the process $H^+ + Li$ with the energy ranging from 10 keV/u to 10 MeV/u, and the results were compared with the experimental results,[35] as shown in Fig. 6. The results demonstrate that TCS for the H^++Li system was in good agreement with the experimental data. The same methods are adopted to the process $H^+ + B^{2+}$. Figure 7 displays the total cross sections of the impact ionization from 1s and 2s sub-shells for B^{2+} impacted by H^+ using the CDW-EIS and M-FEPA methods with the energy ranging from 10 keV/u to 10 MeV/u, respectively. In order to ensure the accuracy of the calculation, the scaled theoretical results for the collision ionization of Li by H^+ are also plotted in Fig. 7. For the high-energy projectile, the ionization cross section for B^{2+} target approaches the scaled cross section for the lithium target, which is well consistent with the scaling law based on FBA.[5] Hence, the data for $H^+ + B^{2+}$ in this paper are reliable. In Fig. 7, comparison of the TCS resulting from M-FEPA and CDW-EIS demonstrates that the difference between the total cross sections obtained from M-FEPA and CDW-EIS is less than 30% in the calculated energy range (for 1s sub-shell, the energy is from 50 keV/u to 10 MeV/u; for 2s sub-shell, the energy is from 500 keV/u to 10 MeV/u), and thus the simple M-FEPA model can give a good estimation of TCS for B^{2+} by proton impact in this case; for the low-energy projectile case, the results of the M-FEPA model cannot be given, as shown by Eq. (14); and the higher energy impact case is not considered in this paper. Comparing the TCS from 1s sub-shell with that from the 2s sub-shell, we find that the ionization from 2s sub-shell is dominant because of its lower ionization energy, especially in the case of the low projectile energy, and almost

accounts for all contributions to the TCS, as shown in the insert of Fig. 7. With the projectile energy increasing, the ionization from the 1s sub-shell becomes more and more important. Finally, the percentages of the partial cross sections from the 1s and 2s sub-shells are basically invariant, as the curve becomes flat. Besides, the TCS has a maximum, which is related to the position where the projectile velocity υ_P approaches the averaged velocity $\bar{\upsilon}_e$ of the initial bound electron relative to the target.[19,37] That is to say, when $\upsilon_P > \bar{\upsilon}_e$ (the high-energy projectile), the ionization cross sections decrease with increasing velocity projectile. When $\upsilon_P < \bar{\upsilon}_e$ (the low-energy projectile), the cross sections decrease with decreasing projectile velocity. This can be proved as follows.

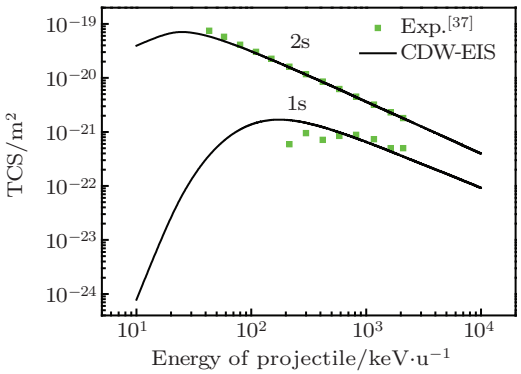


Fig. 6. (color online) Total cross sections from the 1s and 2s orbitals as functions of the projectile energy for the H^++Li system.

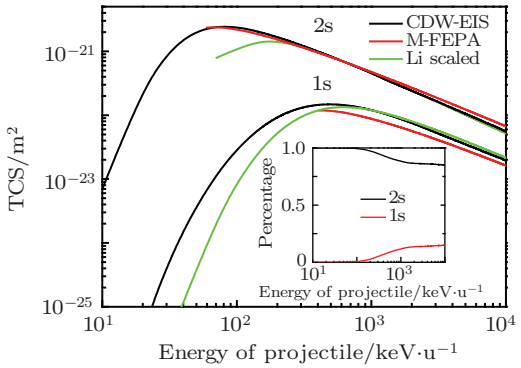


Fig. 7. (color online) Total cross sections from the 1s and 2s orbitals as a function of the projectile energy. Green line: the scaled results from the collision of H^+ with Li,[5] where the cross section is multiplied by $Z_{T'}^{-4}$ ($Z_{T'}^{-4} = \tilde{Z}_{B^{2+}}/\tilde{Z}_{Li} = 1.8854$) and the projectile energy is multiplied by $Z_{T'}^2$. The insert shows the percentages of the partial cross sections from the 1s and 2s sub-shells in the calculated energy range.

The single-differential cross sections (SDCS) from the 1s orbital as a function of the energy of the ejected electron are calculated using Eq. (8) (CDW-EIS), as shown in Fig. 8, at the projectile energy of 100, 200, 500, 1000, 2000, and 5000 keV/u, respectively. Figure 8 shows that the area under the SDCS curve with the projectile energy $E_P = 500$ keV/u ($\upsilon_P \approx \bar{\upsilon}_e$) is the largest, as shown in Fig. 7. When $E_P < 500$ keV/u ($\upsilon_P > \bar{\upsilon}_e$), the area under the SDCS curve decreases with decreasing projectile energy, while when $E_P > 500$ keV/u ($\upsilon_P < \bar{\upsilon}_e$), the area under the SDCS curve decreases as the projectile energy increases. This demonstrates that the collision mechanism depends on the relation between υ_P and $\bar{\upsilon}_e$. For $E_P < 500$ keV/u, it is marked in Fig. 8 that there are clear turning points whose locations correspond to the ECC ionization (for example, $\varepsilon_k \approx 54$ eV when $E_P = 100$ keV/u). With the projectile energy increasing, it is also noted that the turning points corresponding to the ECC ionization gradually disappear, and that the other turning points appear, the locations of which correspond to the BE ionizations (for example, $\varepsilon_k \approx 10893$ eV when $E_P = 5000$ keV/u). This denotes that the ECC ionization mechanism is proved to be important in the moderate- and low-energy collision ranges, and the BE ionization is obvious for the high-energy incident projectile impact as mentioned in Subsection 3.1 and 3.2. But as a whole, the SC ionization governs the total ionization cross sections because most electrons are produced in glancing collisions. Moreover, the higher energies of the incident projectile are, the greater the contributions from SC ionization to TCS are.[19]

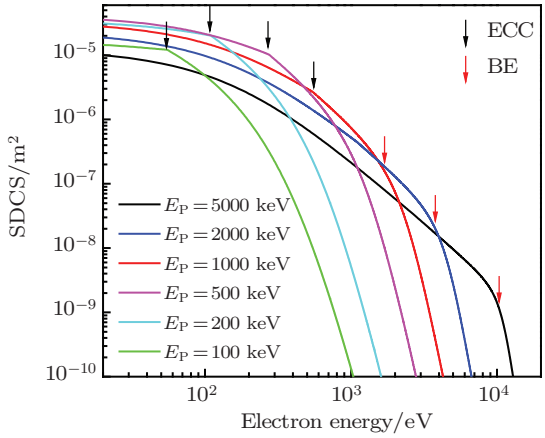


Fig. 8. (color online) Single-differential cross sections of the 1s electron as a function of the energy of ejection electrons for different projectile energies. The black (red) arrows indicate the positions of ECC (BE).

4. Summary

The ionization process of B^{2+} by H^+ impact has an important significance in ICF experimental research. In the present work, the total, single-differential, and double-differential cross sections from 1s and 2s sub-shells for B^{2+} ion are investigated by adopting the CDW-EIS. In order to deeply analyze various ionization mechanisms, M-FEPA results are also given. The ECC ionization mechanism is proved to be important in the moderate- and low-energy collision ranges; the BE ionization mechanism is obvious for the high-energy incident projectile. By comparing with the results of CDW-EIS, we prove again that TCS and SDCS can be well evaluated by adopting the M-FEPA model for the high-energy incident case. Furthermore, the M-FEPA model reproduces

the essential features of BE bump in DDCS, and the BE ionization mechanism is discussed in detail. Especially, the DDCS and SDCS from the 2s orbital show a high-energy hip, which is different from those for the 1s orbital. Moreover, based on Ref. [1], the Compton profiles of B^{2+} for 1s and 2s orbitals are given, and the hips in the DDCS and SDCS from the 2s orbital are explained.

Acknowledgement

The authors thank Prof. Wang Jian-Guo (Beijing Institute of Applied Physics and Computational Mathematics) for useful discussion and suggestions.

References

[1] Biggs F, Mendelssohn L B and Mann J B 1975 *At. Data Nucl. Data Tables* **16** 201
[2] Ovchinnikov S Yu, Ogurtsov G N, Macek J H and Gordeev Yu S 2004 *Phys. Rep.* **389** 119
[3] Liu H P, Chen X M, Ouyang X P, Xi F Y and Su G H 2010 *Chin. Phys. B* **19** 063404
[4] Wang F and Wang M M 2011 *Chin. Phys. B* **20** 113402
[5] Madison D H 1973 *Phys. Rev. A* **8** 2449
[6] Schultz D R, Meng L and Olson R E 1992 *J. Phys. B* **25** 4601
[7] Liu L, Wang J G and Janev R K 2008 *Phys. Rev. A* **77** 042712
[8] Liu L, Liu C H, Wang J G and Janev R K 2011 *Phys. Rev. A* **84** 032710
[9] Liu L and Wang J G 2007 *Chin. Phys. Lett.* **24** 3115
[10] Cheshirec I M 1964 *Proc. Phys. Soc.* **84** 89
[11] Crothers D S F and McCann J F 1983 *J. Phys. B* **16** 3229
[12] Fainstein P D, Ponce V H and Rivarola R 1991 *J. Phys. B* **24** 3091
[13] McCartney M and Crothers D S F 1993 *J. Phys. B* **26** 4561
[14] Fiori M R, Ginette J, Bielschowsky C E and Cravero W 2001 *Phys. Rev. A* **64** 012705
[15] Bethe H and Ann 1930 *Ann. Phys.* **397** 325
[16] Crooks G B and Rudd M E 1970 *Phys. Rev. Lett.* **25** 1599
[17] Rudd M E and Jorgensen T J 1963 *Phys. Rev.* **131** 666
[18] Meckbach W, Focke P J, Goñi A R and Suárez S 1986 *Phys. Rev. Lett.* **57** 1587
[19] Stolterfoht N, DuBois R D and Rivarola R D 1997 *Electron Emission in Heavy Ion–Atom Collisions* (Heidelber: Springer-Verlag)
[20] Huang J, Wan B N, Li J G, Gong X Z, Zhang X D, Wu Z W, Zhou Q and the HT-7 team 2006 *Nucl. Fusion* **46** 262
[21] Janev R K 1992 *Atomic and Plasma-Material Interaction Data for Fusion* (Supplement to the Journal of Nuclear Fusion) (Vienna: International Atomic Energy Agency) **3** 87
[22] Liu L, Jakimovski D, Wang J G and Janev R K 2010 *J. Phys. B* **43** 144005
[23] Berengut J C, Loch S D, Pindzola M S, Ballance C P and Griffin D C 2007 *Phys. Rev. A* **76** 042704
[24] Crandall D H, Phaneuf R A, Gregory D C, Howald A M, Mueller D W, Morgan T J and Dunn G H 1986 *Phys. Rev. A* **34** 1757
[25] Muller A, Schippers S, Phaneuf R A, Scully S W J, Aguilar A, Cisneros C, Gharaibeh M F, Schlachterand A S and McLaughlin B M 2010 *J. Phys. B* **43** 135602
[26] Tseng H C and Lin C D 2000 *Phys. Rev. A* **61** 034701
[27] Das M, Purkait M and Mandal C R 1998 *J. Phys. B* **31** 4387
[28] Schultz D R, Krstic P S and Reinhold C O 1996 *Phys. Scr.* **T62** 69
[29] McSherry D M, O'Rourke S F C and Crothers D S F 2003 *Comput. Phys. Commun.* **155** 144
[30] Clementi E and Roetti C 1974 *At. Data Nucl. Data Tables* **14** 177
[31] Bates D R and McCarroll R 1958 *Proc. R. Soc. Lond. A* **245** 175
[32] Bransden B H and McDowell M R C 1992 *Charge Exchange and the Theory of Ion-Atom Collisions* (Oxford: Clarendon Press)
[33] Bell F, Böckl H, Wu M Z and Betz H D 1983 *J. Phys. B* **16** 187
[34] Stolterfoht N, Chesnel J Y and Grether M 1999 *Phys. Rev. A* **59** 1262
[35] Fainstein P D, Ponce V H and Rivarola R D 1991 *J. Phys. B* **24** 3091
[36] Rudd M E, Kim Y K, Madison D H and Gay T J 1992 *Rev. Mod. Phys.* **64** 441
[37] Ning Y, He B, Liu C L, Yan J and Wang J G 2005 *Phys. Rev. A* **72** 022702
[38] Shah M B, Elliott D S and Gilbody H B 1985 *J. Phys. B* **18** 4245